



Solar Longitude Distribution of High-energy Proton Flares: Fluences and Spectra

E. W. Cliver^{1,2} , F. Mekhaldi³, and R. Muscheler³¹School of Physics & Astronomy, University of Glasgow, Glasgow G12 8QQ, UK²National Solar Observatory, 3665 Discovery Drive, Boulder, CO, 80303, USA³Department of Geology—Quaternary Sciences, Lund University, SE-22362 Lund, Sweden

Received 2020 June 29; revised 2020 August 7; accepted 2020 August 7; published 2020 September 1

Abstract

The distribution of the longitudes of solar flares associated with the high-energy proton events called ground level events (GLEs) can be approximated by a Gaussian with a peak at \sim W60, with a full range from \sim E90 to \sim W150. The longitudes of flares associated with the top third (24 of 72) of GLEs in terms of their $>$ 430 MeV fluences (F_{430}) are primarily distributed over E20–W100 with a skew toward disk center. This 120° span in longitude is comparable to the latitudinal spans of powerful coronal mass ejections (CMEs) from limb flares. Only 5 of 24 strong GLEs are located within the W40–80 zone of good magnetic connection to Earth. GLEs with hard spectra, i.e., a spectral index $SI_{30/200} (= \log(F_{30}/F_{200})) < 1.5$, also tend to avoid W40–80 source regions. Three-fourths of such events (16 of 21) arise in flares outside this range. The above tendencies favor a CME-driven shock source over a flare-resident acceleration process for high-energy solar protons. GLE spectra show a trend, with broad scatter, from hard spectra for events originating in eruptive flares beyond the west limb to soft spectra for GLEs with sources near central meridian. This behavior can be explained in terms of: (1) dominant near-Sun quasi-perpendicular shock acceleration of protons for far western ($>$ W100) GLEs; (2) quasi-parallel shock acceleration for well-connected (W40–80) GLEs, and (3) proton acceleration/trapping at CME-driven bow shocks from central meridian (E20–W20) that strike the Earth.

Unified Astronomy Thesaurus concepts: Solar energetic particles (1491); Solar flares (1496); Solar coronal mass ejections (310); Solar coronal mass ejection shocks (1997)

1. Introduction

The high-energy proton events monitored by the worldwide network of ground-based neutron monitors (NMs; Simpson et al. 1953; Bieber & Evenson 1995; Mavromichalaki et al. 2011) are termed ground level events (GLEs). The effective energy threshold for GLEs is 1 GV in rigidity (430 MeV in energy; Mishev et al. 2013). GLEs were first detected in 1942 by ionization chambers (Lange & Forbush 1942; Forbush 1946). To date, 72 GLEs have been observed.⁴

Until recently, the principal measure of GLE strength was the largest percentage increase above background observed at any sea-level station (e.g., McCracken et al. 2012; Poluianov et al. 2017). This intensity measure is not ideal because it depends on event timing relative to the location of a changing network of monitors. Because of the lack of a well-defined parameter for GLE strength, distributions of the solar longitudes of GLE-associated flares typically include all GLEs, regardless of size, resulting in a broad Gaussian centered at \sim W60 (e.g., Figure 1 in Smart & Shea 1996), near the nominal \sim W55 footpoint (based on the Sun’s rotation rate and the average speed of the solar wind) of the magnetic field-line connecting to Earth. Data now exist to examine the solar longitude distribution of GLEs in greater detail. Tylka & Dietrich (2009) undertook a systematic evaluation of NM and space-based data to construct spectra for all GLEs that were sufficiently large. This work was recently updated and more

thoroughly documented by Raukunen et al. (2018) to provide a homogeneous database of GLEs, permitting the determination of proton fluences at all energies.

In this study we use this database to examine where the strongest (and weakest) GLEs in terms of $>$ 430 MeV fluence (F_{430}) originate on the Sun. We also examine the variation of GLE spectra, as characterized by $\log(F_{30}/F_{200})$, with source longitude. Our analysis is presented in Section 2 and results are discussed in Section 3.

2. Analysis

2.1. Data

Table 1 gives the dates, solar flare coordinates, proton fluences (F_{30} , F_{200} , and F_{430}), and the spectral index $SI_{30/200} (= \log(F_{30}/F_{200}))$ determined from the spectral parameters given in Raukunen et al. (2018) for 59 of the 72 GLEs. The Raukunen et al. analysis did not consider the first four GLEs (all observed before the neutron monitor era), the most recent GLE on 2017 September 10, and eight other GLEs for which the proton fluences were considered too small to make reliable spectral fits. In our fluence analysis, we divided GLEs into the top third (24 GLEs), middle third, and bottom third in terms of their $>$ 430 MeV fluence. We assigned GLE Nos. 1–4 to the top third. Because of their less sensitive mode of observation, the first four GLEs are considered to be among the largest observed (Duggal 1979; Smart & Shea 1991; Shea & Smart 2019). We took the eight events not analyzed by Raukunen et al. (2018) to be among the smallest third. Quoting from their paper, “...eight [GLEs] had too small fluences for the [spectral fits] to be reliable.” Based on comparison with other GLEs on the Oulu website, we assigned GLE No. 72 (Mishev et al. 2018) to the middle third of events. For six of the GLEs (No. 42: 1989

⁴ <https://gle.oulu.fi/#/>; www.nmdb.eu/nest/gle_list.php

Table 1
Parameters of GLEs, 1942–2017

No.	Year	Month	Day	F_{30} (cm $^{-2}$)	F_{200} (cm $^{-2}$)	F_{430} (cm $^{-2}$)	SI $_{30/200}$	Location ^a
1	1942	Feb	28	N/A				N07E04
2	1942	Mar	07	N/A				N07W90
3	1946	Jul	25	N/A				N22E15
4	1949	Nov	19	N/A				S02W70
5	1956	Feb	23	1.42E+09	1.21E+08	3.03E+07	1.07	N23W80
6	1956	Aug	31	N/A				N15E15
7	1959	Jul	16	1.03E+09	1.62E+07	1.16E+06	1.80	N16W31
8	1960	May	04	4.84E+06	5.31E+05	1.50E+05	0.96	N13W90
9	1960	Sep	03	3.59E+07	1.48E+06	1.38E+05	1.39	N18E88
10	1960	Nov	12	3.17E+09	6.40E+07	6.99E+06	1.70	N27W04
11	1960	Nov	15	1.72E+09	3.03E+07	3.47E+06	1.75	N25W35
12	1960	Nov	20	4.46E+07	1.90E+06	2.16E+05	1.37	N25W113
13	1961	Jul	18	3.01E+08	6.42E+06	4.54E+05	1.67	S07W59
14	1961	Jul	20	N/A				S06W90
15	1966	Jul	07	N/A				N35W48
16	1967	Jan	28	N/A				N22W154
17	1967	Jan	28	8.52E+07	4.36E+06	7.41E+05	1.29	N22W154
18	1968	Sep	29	N/A				N17W51
19	1968	Nov	18	1.53E+08	1.73E+06	1.18E+05	1.94	N21W87
20	1969	Feb	25	N/A				N13W37
21	1969	Mar	30	3.25E+07	1.66E+06	2.54E+05	1.29	N19W106
22	1971	Jan	24	3.42E+08	3.29E+06	2.34E+05	2.02	N19W49
23	1971	Sep	01	1.70E+08	9.04E+06	9.56E+05	1.27	S11W120
24	1972	Aug	04	7.84E+09	1.41E+07	4.44E+05	2.74	N14E08
25	1972	Aug	07	3.01E+08	3.05E+06	2.31E+05	1.99	N14W37
26	1973	Apr	29	7.71E+06	2.32E+05	3.36E+04	1.52	N13W73
27	1976	Apr	30	2.74E+07	6.96E+05	5.99E+04	1.59	S08W46
28	1977	Sep	19	4.76E+07	6.75E+05	6.01E+04	1.85	N08W57
29	1977	Sep	24	2.53E+07	1.38E+06	2.30E+05	1.26	N10W120
30	1977	Nov	22	6.41E+07	2.01E+06	2.91E+05	1.50	N24W40
31	1978	May	07	1.57E+07	4.61E+05	8.56E+04	1.53	N23W72
32	1978	Sep	23	4.78E+08	2.56E+06	2.23E+05	2.27	N35W50
33	1979	Aug	21	N/A				N17W40
34	1981	Apr	10	N/A				N07W36
35	1981	May	10	2.93E+07	2.74E+05	2.86E+04	2.03	N03 W75
36	1981	Oct	12	2.05E+08	1.38E+06	1.49E+05	2.17	S18E31
37	1982	Nov	26	2.05E+07	4.59E+05	7.08E+04	1.65	S12W87
38	1982	Dec	07	6.97E+07	1.28E+06	1.93E+05	1.74	S19W86
39	1984	Feb	16	1.73E+07	6.88E+05	7.76E+04	1.40	~W130
40	1989	Jul	25	7.50E+06	4.74E+05	5.43E+04	1.20	N26W85
41	1989	Aug	16	3.07E+08	5.16E+06	4.15E+05	1.77	S15W85
42 <i>P</i>	1989	Sep	29	3.21E+06	3.73E+05	1.38E+05	0.93	~W100
42 ESP	1989	Sep	29	1.38E+09	3.07E+07	4.18E+06	1.65	
42 (<i>P</i> +ESP)	1989	Sep	29	1.38E+09	3.10E+07	4.32E+06	1.65	
43 <i>P</i>	1989	Oct	19	5.95E+08	2.88E+07	2.79E+06	1.31	S25E09
43 ESP	1989	Oct	19	1.96E+09	2.63E+07	3.82E+06	1.87	
43 (<i>P</i> +ESP)	1989	Oct	19	2.56E+09	5.51E+07	6.60E+06	1.67	
44	1989	Oct	22	1.08E+09	1.58E+07	7.82E+05	1.83	S27W32
45	1989	Oct	24	5.37E+08	2.16E+07	3.35E+06	1.40	S29W57
46	1989	Nov	15	5.20E+06	3.15E+05	4.18E+04	1.22	N11W28
47	1990	May	21	4.33E+07	1.44E+06	2.21E+05	1.48	N34W37
48	1990	May	24	4.74E+07	2.34E+06	2.89E+05	1.31	N36W76
49	1990	May	26	2.03E+07	1.60E+06	2.03E+05	1.10	~W100
50	1990	May	28	2.62E+07	1.02E+06	1.16E+05	1.41	~W120
51	1991	Jun	11	3.43E+08	3.94E+06	4.21E+05	1.94	N32W15
52	1991	Jun	15	2.07E+08	4.28E+06	3.81E+05	1.68	N36W70
53	1992	Jun	25	3.77E+07	5.38E+05	5.07E+04	1.85	N10W68
54	1992	Nov	02	3.07E+08	2.77E+06	1.37E+05	2.05	~W100
55	1997	Nov	06	1.55E+08	3.63E+06	3.49E+05	1.63	S18W63
56	1998	May	02	1.73E+07	5.95E+05	5.60E+04	1.46	S15W15
57	1998	May	06	7.82E+06	1.57E+05	1.19E+04	1.70	S15W64
58 <i>P</i>	1998	Aug	24	1.05E+07	3.00E+05	4.88E+04	1.54	N35E09
58 ESP	1998	Aug	24	2.47E+07	8.64E+04	6.04E+03	2.46	

Table 1
(Continued)

No.	Year	Month	Day	F_{30} (cm ⁻²)	F_{200} (cm ⁻²)	F_{430} (cm ⁻²)	SI _{30/200}	Location ^a
58 (<i>P</i> +ESP)	1998	Aug	24	3.52E+07	3.86E+05	5.48E+04	1.96	
59 <i>P</i>	2000	Jul	14	8.72E+08	1.95E+07	9.76E+05	1.65	N22W07
59 ESP	2000	Jul	14	2.15E+09	1.44E+07	7.42E+05	2.17	
59 (<i>P</i> +ESP)	2000	Jul	14	3.02E+09	3.39E+07	1.72E+06	1.95	
60	2001	Apr	15	1.52E+08	8.05E+06	1.14E+06	1.28	S20W84
61	2001	Apr	18	4.31E+07	1.25E+06	1.45E+05	1.54	~W115
62 <i>P</i>	2001	Nov	04	2.33E+08	2.43E+06	1.33E+05	1.98	N07W19
62 ESP	2001	Nov	04	2.19E+09	9.11E+06	2.14E+05	2.38	
62 (<i>P</i> +ESP)	2001	Nov	04	2.42E+09	1.15E+07	3.47E+05	2.32	
63	2001	Dec	26	7.65E+07	1.34E+06	8.63E+04	1.76	N08W54
64	2002	Aug	24	5.11E+07	8.13E+05	6.11E+04	1.80	S02W81
65 <i>P</i>	2003	Oct	28	5.79E+08	6.24E+06	3.72E+05	1.97	S16E08
65 ESP	2003	Oct	28	1.54E+09	8.87E+06	3.34E+05	2.24	
65 (<i>P</i> +ESP)				2.12E+09	1.51E+07	7.06E+05	2.15	
66	2003	Oct	29	4.41E+08	8.17E+06	6.10E+05	1.73	S15W02
67	2003	Nov	02	1.61E+08	1.42E+06	1.03E+05	2.06	S14W56
68	2005	Jan	17	3.55E+08	2.10E+06	7.74E+04	2.23	N13W23
69	2005	Jan	20	3.29E+08	2.21E+07	2.89E+06	1.17	N12W58
70	2006	Dec	13	1.55E+08	5.53E+06	5.16E+05	1.45	S06W23
71	2012	May	17	2.42E+07	9.86E+05	1.10E+05	1.39	N11W76
72	2017	Sep	10	N/A				S09W92

Note.

^a Data sources: Cliver et al. (1982), Cliver (2006), Gopalswamy et al. (2012, 2013, 2018).

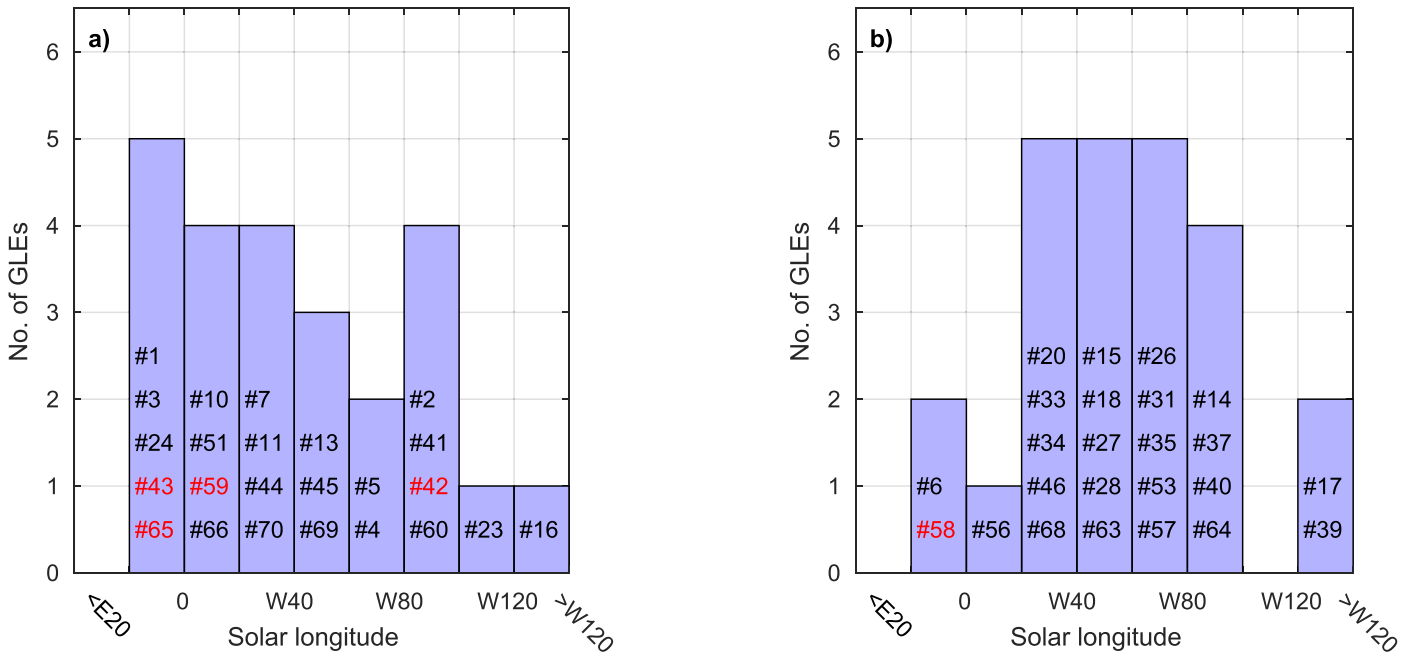


Figure 1. Histograms of the solar longitudes of (a) the strongest third of GLEs in terms of F_{430} from 1942 to 2012 and (b) the weakest third of GLEs during this interval. The chronological number of individual GLEs in each bin is indicated, with those for which a delayed ESP component was observed given in red.

September 29; No. 43: 1989 October 19; No. 58: 1998 August 24; No. 59: 2000 July 14; No. 62: 2001 November 4; No. 65: 2003 October 28), Raukunen et al. obtained spectra for both the initial prompt (*P*) component of a GLE and a delayed energetic storm particle (ESP; Rao et al. 1967; Lario & Decker 2002) component. In these cases we give the *P* and ESP components in Table 1, as well as the combined (*P* + ESP) fluences that we used to obtain the log (F_{30}/F_{200}) spectral index. The largest bottom third (middle third) F_{430} event was 2001 December 26 with 8.63×10^4 cm⁻² (1991 June 15 with 3.81×10^5 cm⁻²).

2.2. Analysis

Figures 1(a), (b) contain histograms of F_{430} for the GLEs with the 24 highest and 24 lowest rank order fluences, respectively. The highest-fluence events show a broad distribution from E20 to W100 that is skewed toward disk center, similar to the distribution Smart et al. (2006) obtained for >30 MeV protons. The GLE numbers are given in the histograms, with the two-component (*P* + ESP) events in red. It is likely that GLE Nos. 1 and 3 were also in this category.

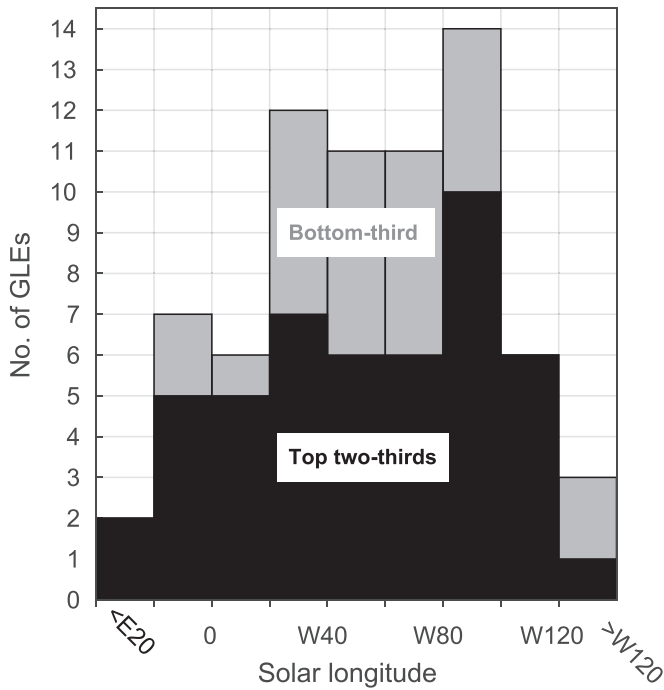


Figure 2. Histogram of the source longitudes of all GLEs. Black shading indicates the top two-thirds of GLEs in terms of F_{430} , with the gray shading denoting the bottom third of GLEs in this parameter.

Removal of the ESP component for the six events for which we have data would change the classification for GLE No. 42, dropping it out of the top third. This event was unusual in that while the other five events were all located within 20° of disk center, the 1989 September GLE is associated with an eruptive flare located at W100.

The histogram in Figure 1(b) shows a broad distribution centered at $\sim W60$ for the solar locations of the third of GLEs from 1942 to 2017 with the lowest F_{430} values. Figure 2 shows that the broad peak in the distribution for all GLEs in the overarching histogram is primarily due to the concentration of small GLEs in the W20–100 range.

Figure 3 is a plot of the proton spectral index $\log(F_{30}/F_{200})$ versus solar flare longitude (Kovaltsov et al. 2014; Asvestari et al. 2017) for the 59 GLEs from 1956 to 2012 analyzed by Raukunen et al. (2018). These GLEs span a total longitude range of $\sim 240^\circ$, from E88 to W154. The events are color-coded by their F_{430} fluence ranking as follows: top third (magenta), middle third (black), and bottom third (green). The dashed horizontal line bounds hard spectrum events with $\log(F_{30}/F_{200})$ values < 1.5 , and the two dashed vertical gray lines mark the zone of favorable magnetic connection from W40 to 80. The solid line is an ordinary least-squares fit to the scatter showing spectral hardening (reduction of $\log(F_{30}/F_{200})$) as one moves westward from solar disk center. In particular, all eight far west GLEs, i.e., those originating at $>W100$, have spectral indices $\lesssim 1.5$ (c.f., Figure 10 in Van Hollebeke et al. 1975 at lower energies). The hardest spectra events tend to avoid the W40–80 zone of good magnetic connection. Of the 21 GLEs with $\log(F_{30}/F_{200}) < 1.5$, only 5 originated from W40 to 80, with 11 associated with flares located $>W80$.

The median GLE $SI_{30/200}$ value increases from ~ 1.35 for $>W100$ events to ~ 1.65 for events from the W40–80 zone of good magnetic connection to ~ 1.95 for GLEs from central meridian (E20–W20). The 13 central meridian GLEs in Table 1

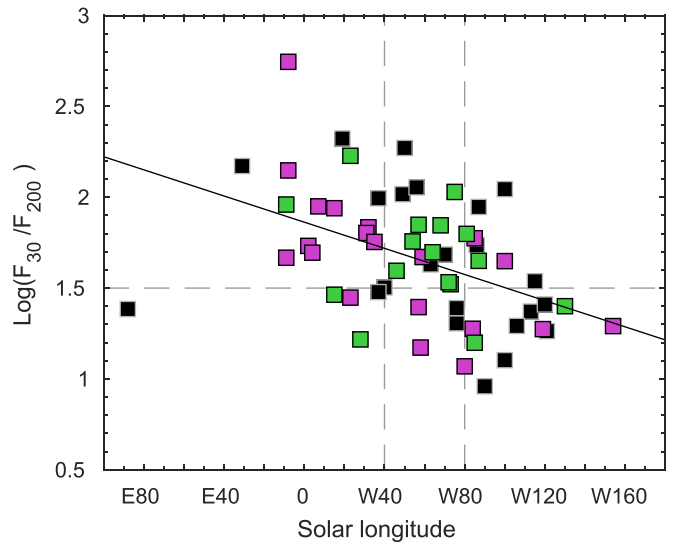


Figure 3. Plot of the proton spectral index $\log(F_{30}/F_{200})$ vs. longitude for 59 GLEs from 1956 to 2012 analyzed by Raukunen et al. (2018). The events are color-coded according to the rank order of their >430 MeV fluence: top third (magenta), middle third (black), and bottom third (green). The gray horizontal dashed line is drawn at a spectral index of 1.5, and the vertical dashed lines mark the $\sim W40$ –80 region of good magnetic connection to Earth. An ordinary least-squares fit (solid line) is shown. The two GLEs at W120 with $SI_{30/200} \sim 1.25$ are slightly offset in longitude for visibility in the plot.

are strongly associated with “fast transit” CMEs, i.e., CMEs with intervals from eruptive flare onset to a geomagnetic storm sudden commencement (SC; shock arrival) at Earth of $\lesssim 20$ hr (Cliver et al. 1990a, 1990b), or 30 hr interval (Gopalswamy et al. 2005) as used here. Table 2(a) gives the dates, flare onset times, transit time interval, F_{430} size rank (in thirds), $SI_{30/200}$ value, ESP occurrence (yes/no), and references for the E20–W20 events in Table 1. Only four of the Table 2(a) events have transit times longer than 30 hr (range from 32 to 38.1 hr). At least 7 of the 12 soft-spectrum GLEs ($SI_{30/200} \gtrsim 1.7$) from E20–W20 longitudes are associated with shocks at Earth. In addition to the five such events for which Raukunen et al. (2018) computed a separate ESP spectrum, the 1972 August 4 (Pomerantz & Duggal 1974) and 2003 October 29 (Gopalswamy et al. 2005, their Table 3 and Figure 9) had shock-related >30 MeV proton enhancements at Earth. Pomerantz & Duggal (1974) attributed the steep spectrum ($SI_{30/200} = 2.74$) of the 1972 August GLE, as well as GLE No. 7 (1959 July 16; W31; $SI_{30/200} = 1.8$), to proton acceleration by converging shocks in interplanetary space. The central meridian GLEs on 1960 November 12 and 2000 July 14 may have been similar in this regard. In both cases one or more SCs were recorded near the time of the GLE-parent flare. The strong central meridian GLEs associated with fast transit shocks in 1942 and 1946 are other candidates for ESP association. For the six GLEs with defined ESP components, the spectra of the combined ($P + \text{ESP}$) GLE are softer than the initial prompt component: 1989 September 29 ($\sim W100$; $P + \text{ESP} = 1.65$, $P = 0.93$); 1989 October 19 (E09; 1.67, 1.31); 1998 August 24 (E09; 1.96, 1.54); 2000 July 14 (W07; 1.95, 1.65); 2001 November 4 (W19; 2.32, 1.98); 2003 October 28 (E08; 2.15, 1.97). $SI_{30/200}$ values for the ESP events from the five central meridian GLEs in this list ranged from 1.87 to 2.46. For four of these five cases, the ESP contribution to the >200 and >430 MeV fluences was significant, typically from $\sim 40\%$ to

Table 2
Parameters of GLEs Associated with (a) Central Meridian (E20–W20) Eruptive Flares and (b) GLEs Associated with Far West (>W100) Eruptions

(a) Date	Longitude (UT)	Flare Onset ^a (hr)	Transit Time ^b	F_{430} Rank	SI _{30/200}	ESP?	References ^c
1942 Feb 28	E04	<11:00	20.5	Top	N/A	yes?	(1)
1946 Jul 25	E15	15:04	27.6	Top	N/A	yes?	(1)
1956 Aug 31	E15	12:26	38.1	Bottom	N/A	no?	(2)
1960 Nov 12	W04	13:15	21.2 ^d	Top	1.70	yes?	(3)
1972 Aug 4	E08	6:20	14.6	Top	2.74	yes	(4)
1989 Oct 19	E09	12:29	28.5	Top	1.67	yes	(5)
1991 Jun 11	W15	2:09	32	Top	1.94	no? ^e	(6)
1998 May 2	W15	13:31	28.2	Bottom	1.46	no	(6)
1998 Aug 24	E09	21:50	33	Bottom	1.96	yes	(7)
2000 Jul 14	W07	10:24	27.9	Top	1.95	yes	(8)
2001 Nov 4	W19	16:03	33.8	Middle	2.32	yes	(7)
2003 Oct 28	E08	11:06	18.9	Top	2.15	yes	(8)
2003 Oct 29	W02	20:41	19.7	Top	1.73	yes	(9)
(b) Date	Longitude (UT)	Flare Onset ^f (hr)	Transit Time	F_{430} Rank	SI _{30/200}	ESP?	References ^g
1960 Nov 20	W113	20:17	10.3 ^h	Middle	1.37	Modulation	(1)
1967 Jan 28	W154	7:54	... ⁱ	Top	1.29	...	
1969 Mar 30	W106	2:47	...	Middle	1.29	...	
1971 Sep 1	W120	19:34	69.2	Top	1.27	Modulation ^j	(2)
1977 Sep 24	W120	5:54	... ^k	Middle	1.26	...	
1984 Feb 16	~W130	~9:00	...	Bottom	1.40	...	
1990 May 28	~W120	4:33	52.5	Middle	1.41	Modulation ^l	(3)
2001 Apr 18	~W115	2:14	85.8	Middle	1.54	no ^m	(3)

Notes.

^a Onset times are based on the principal source (first reference listed) for each event and are variously based on H α , radio, soft X-ray, and CME observations.

^b Interval between flare onset time and sudden commencement unless otherwise noted.

^c References: (1) Cliver et al. (1990b) and references therein; (2) Mayaud (1973), Švestka & Simon (1975); (3) Gopalswamy et al. (2005) and references therein, Obayashi (1962); (4) Pomerantz & Duggal (1974); Cliver et al. (1990b), Kallenrode & Cliver (2001); (5) Cliver et al. (1990b), Raukunen et al. (2018); (6) flare onset from <https://www.ngdc.noaa.gov/stp/space-weather/solar-data/solar-features/solar-flares/x-rays/goes/xrs/>, >30 MeV event time profile from <https://www.ngdc.noaa.gov/stp/satellite/goes/dataaccess.html>, SC from Solar-Geophysical Data (SGD); (7) flare onset from NOAA SXR, SGD, Raukunen et al. (2018); (8) Gopalswamy et al. (2005), Raukunen et al. (2018); (9) Gopalswamy et al. (2005).

^d Ellison et al. (1961) and Obayashi (1962) report a large amplitude SC at ~10:22 UT on November 13 that is not included in Mayaud's (1973) list.

^e Modulation of the >30 MeV proton time profile is not clearly related to the SC.

^f All onset times from Cliver et al. (1982) and Cliver (2006).

^g References: (1) SC from Švestka & Simon (1975), no SC reported by Mayaud (1973) on November 21, GLE time profile from <https://gle oulu.fi>; (2) SC and >30 MeV time profile from SGD; (3) SC and >30 MeV profile from NOAA (see above).

^h The shock is presumably not associated with the listed flare but modulates the GLE time profile at certain stations.

ⁱ Mbour reported an SC at 21:18 UT on March 30.

^j The shock ends a slight enhancement on the >30 MeV time profile.

^k SCs reported at Hyderabad and Port Moresby at 07:32 UT on September 26 but an SC is not included in the listing of Romaná.

^l The >30 MeV time profile drops by a factor of ~3 at the shock, near the end of the event.

^m Modulation of >30 MeV time profile not related to time of SC.

60% of the total. In all five cases, the ESP contribution to F_{30} was dominant by factors of ~2–3 or more. In contrast, only three of the eight far western (>W100) GLEs in Table 1 had confirmed associated SCs and the delay from the flare for these three events ranged from ~50 to 80 hr (Table 2(b)). Effects on the >30 MeV proton time profile at the time of shock arrival at Earth for these events were weak or absent.

3. Discussion

After an extended debate (e.g., Reames 2015), it is generally accepted that large solar proton events are primarily due to diffusive shock acceleration (DSA; Desai & Giacalone 2016) at

shocks driven by coronal mass ejections (CMEs) rather than to a flare-resident process. If there is a remaining area of uncertainty, it is for the highest-energy proton events (McCracken et al. 2008; Moraal & McCracken 2012; Klein et al. 2014; Cliver 2016; Klein & Dalla 2017). The comprehensive characterization of GLEs by Raukunen et al. (2018) following the work of Tytka & Dietrich (2009) permits further investigation of this question.

The distribution of source longitudes for the highest-fluence GLEs in Figure 1(a) argues against a picture in which high-energy protons are accelerated locally in a solar flare. In such a picture, one would expect the strongest GLEs to be preferentially produced near W60 with proton fluences falling

off with distance from this location. Instead, the distribution in Figure 1(a) is skewed toward disk center with only 5 of 24 such GLEs originating from W40 to 80. The broad distribution of source longitudes in Figure 1(a), with the bulk of large GLEs having sources from \sim E20 to W100, corresponds to the $\gtrsim 120^\circ$ angular span in latitude for powerful CMEs originating at the solar limbs (Gopalswamy et al. 2015), supporting the CME-driven shock picture for high-energy proton acceleration. Figure 2 shows that it is the third of GLEs with the lowest F_{430} values that are primarily responsible for the broad W20–100 peak in the overall distribution of source longitudes. Apparently, these weaker GLEs (Figure 1(b)) benefit from the proximity of their source to the \sim W55 footpoint of the magnetic field-line connected to Earth.

In the CME-driven shock picture of high-energy proton acceleration, we would expect GLE spectra to result from some combination of quasi-perpendicular and quasi-parallel shock acceleration. Figure 3 gives hints as to how this apportionment occurs with source longitude. Quasi-perpendicular shock acceleration, in which the shock is propagating perpendicularly to the ambient magnetic field, is a special case of DSA (Jokipii 1982, 1987; Tylka et al. 2005; Zank et al. 2006) that produces a harder spectrum than quasi-parallel acceleration. The hard spectra of the eight ($>$ W100) events in Figure 3 are interpreted as a signature of dominant quasi-perpendicular acceleration by a shock driven across the face of the Sun by the lateral expansion of a CME to reach the magnetic field-line to Earth rooted $>40^\circ$ in longitude from the flare site. The corresponding radial motion of the CME responsible for quasi-parallel shock acceleration is directed away from the Earth–Sun line and the Archimedean-spiral magnetic field line to Earth. As a result, the bow shock driven outward by the CME is unlikely to strike the Earth (see, e.g., Figure 2 in Cane et al. 1988) or to remotely produce a strong proton response there by accelerating protons on Earth-directed field lines (Table 2(b)). High-energy protons produced near the Sun at the nose of the bow shock (e.g., Gopalswamy et al. 2013) for a far west GLE will sweep past 1 au ahead of the Earth in its orbit.

The softening of the GLE proton spectrum at Earth as one moves from the west limb toward \sim W60 can be explained in terms of an increasing (decreasing) contribution from quasi-parallel (quasi-perpendicular) shock acceleration of high-energy protons. The quasi-perpendicular contribution to GLEs should have its minimum at \sim W60. This follows from the location of the eruptive flare under, rather than flanking, open field lines to Earth and is consistent with the relative lack of hard-spectra GLEs from W40 to 80 (Figure 3). GLEs originating east of W40, like those west of this longitude zone, can have a quasi-perpendicular component, and there are six GLEs in this zone with hard spectra ($SI_{30/200} \leq 1.5$). The bulk (15/21) of GLEs east of W40, however, have $SI_{30/200} > 1.5$, suggesting dominant quasi-parallel shock acceleration of protons. In contrast to eruptive flares arising from $>$ W100, a bow shock from a central meridian (E20–W20) GLE-parent flare has a high probability of being detected in situ at Earth (Table 2(a)). During its journey to Earth, it can (1) accelerate protons on the field lines to Earth on its western flank because of the eastward curvature of the interplanetary magnetic field (while those accelerated near the Sun at the shock nose will pass behind the Earth), and/or (2) accelerate protons as it converges with earlier slower CMEs (e.g., Pomerantz & Duggal 1974; Kallenrode & Cliver 2001). At

Earth, it can produce an ESP event due either to local acceleration (Reames 2013) or a magnetically trapped population (Lario & Decker 2002). Because the CME-driven shock will decelerate and weaken over time, proton acceleration at the bow shock will produce a progressively softer spectrum at Earth during the time that the shock is connected to the magnetic spiral to Earth—a time that will naturally be greater for central meridian eruptions than for those from beyond the west limb. The resulting soft proton spectra for these various processes make bow shocks from central meridian CMEs the principal candidate for the cause of the broad peak in $SI_{30/200}$ from \sim E20 to W20 in the scatter plot in Figure 3.

E.W.C. and F.M. acknowledge participation in the workshop on the Hostile Sun at Nagoya University in 2018 October organized by F. Miyake and I. Usoskin. E.W.C. has benefited from membership in the ongoing ISSI Team on high-energy SPEs led by A. Papaioannou. He thanks L. Fletcher for kindly sponsoring his stay at the University of Glasgow.

ORCID iDs

E. W. Cliver  <https://orcid.org/0000-0002-4342-6728>

References

- Asvestari, E., Willamo, T., Gil, A., et al. 2017, *AdSpR*, **60**, 781
 Bieber, J. W., & Evenson, P. 1995, *ICRC (Rome)*, **4**, 1316
 Cane, H. V., Reames, D. V., & von Roseninge, T. T. 1988, *JGR*, **93**, 9555
 Cliver, E. W. 2006, *ApJ*, **639**, 1206
 Cliver, E. W. 2016, *ApJ*, **832**, 128
 Cliver, E. W., Feynman, J., & Garrett, H. B. 1990a, in *Solar-Terrestrial Predictions*, Vol. 1, ed. R. J. Thompson et al. (Boulder, CO: NOAA), 348
 Cliver, E. W., Feynman, J., & Garrett, H. B. 1990b, *JGR*, **95**, 17103
 Cliver, E. W., Kahler, S. W., Shea, M. A., & Smart, D. F. 1982, *ApJ*, **260**, 362
 Desai, M., & Giacalone, J. 2016, *LRSP*, **13**, 3
 Duggal, S. 1979, *RvGeo*, **17**, 1021
 Ellison, M. A., McKenna, S. S. M. P., & Reid, J. H. 1961, *MNRAS*, **122**, 491
 Forbush, S. E. 1946, *PhRv*, **70**, 771
 Gopalswamy, N., Tsurutani, B., & Yan, Y. 2015, *PEPS*, **2**, 13
 Gopalswamy, N., Xie, H., Akiyama, S., et al. 2013, *ApJL*, **765**, L30
 Gopalswamy, N., Xie, H., Yashiro, S., et al. 2012, *SSRv*, **171**, 23
 Gopalswamy, N., Yashiro, S., Liu, Y., et al. 2005, *JGRA*, **110**, A09S15
 Gopalswamy, N., Yashiro, S., Mäkelä, P., et al. 2018, *ApJL*, **863**, L39
 Jokipii, J. R. 1982, *ApJ*, **255**, 716
 Jokipii, J. R. 1987, *ApJ*, **313**, 842
 Kallenrode, M.-B., & Cliver, E. W. 2001, *ICRC (Hamburg)*, **8**, 3314
 Klein, K.-L., Masson, S., Bouratzis, C., et al. 2014, *A&A*, **572**, A4
 Klein, L., & Dalla, S. 2017, *SSRv*, **212**, 1107
 Kovaltsov, G. A., Usoskin, I. G., Cliver, E. W., Dietrich, W. F., & Tylka, A. J. 2014, *SoPh*, **289**, 4691
 Lange, I., & Forbush, S. E. 1942, *Terr. Mag. Atmos. Electr.*, **47**, 331
 Lario, D., & Decker, R. B. 2002, *GeoRL*, **29**, 1393
 Mavromichalaki, H., Papaioannou, A., Plainaki, C., et al. 2011, *AdSpR*, **47**, 2210
 Mayaud, P. N. 1973, *A Hundred Year Series of Geomagnetic Data, 1868–1967 Indices aa, Storm Sudden Commencements*, Bull (Paris: IAGA), 33
 McCracken, K. G., Moraal, H., & Shea, M. A. 2012, *ApJ*, **761**, 101
 McCracken, K. G., Moraal, H., & Stoker, P. H. 2008, *JGRA*, **113**, 12101
 Mishev, A., Usoskin, I., Raukunen, O., et al. 2018, *SoPh*, **293**, 136
 Mishev, A. L., Usoskin, I. G., & Kovaltsov, G. A. 2013, *JGRA*, **118**, 2783
 Moraal, H., & McCracken, K. G. 2012, *SSRv*, **171**, 85
 Obayashi, T. 1962, in *AFCRL Studies of the November 1960 Solar-Terrestrial Events*, AFCRL-62-441, ed. J. Aarons & S. M. Silverman (Bedford, MA: AFCRL), 1
 Poluianov, S. V., Usoskin, I. G., Mishev, A. L., Shea, M. A., & Smart, D. F. 2017, *SoPh*, **292**, 176
 Pomerantz, M., & Duggal, S. 1974, *JGR*, **79**, 913
 Rao, U. R., McCracken, K. G., & Bukata, R. P. 1967, *JGR*, **72**, 4325
 Raukunen, O., Vainio, R., Tylka, A. J., et al. 2018, *JWSWC*, **8**, A04
 Reames, D. V. 2013, *SSRv*, **175**, 53

- Reames, D. V. 2015, *SSRv*, 194, 303
- Shea, M. A., & Smart, D. F. 2019, ICRC (Madison, WI), 36, 1149
- Simpson, J. A., Fonger, W., & Treiman, S. B. 1953, *PhRv*, 90, 934
- Smart, D. F., & Shea, M. A. 1991, ICRC (Dublin), 3, 101
- Smart, D. F., & Shea, M. A. 1996, *AdSpR*, 17, 113
- Smart, D. F., Shea, M. A., Spence, H. E., & Kepko, L. 2006, *AdSpR*, 37, 1734
- Tylka, A. J., Cohen, C. M. S., Dietrich, W. F., et al. 2005, *ApJ*, 625, 474
- Tylka, A. J., & Dietrich, W. F. 2009, ICRC (Łódź), 31, 0273
- Van Hollebeke, M. A. I., Ma Sung, L. S., & McDonald, F. B. 1975, *SoPh*, 41, 189
- Švestka, Z., & Simon, P. 1975, Catalog of Solar Particle Events 1955–1969 (Dordrecht: D. Reidel)
- Zank, G. P., Li, G., Florinski, V., et al. 2006, *JGRA*, 111, A06108